Pumping-induced regional land subsidence: calibrating a flow and compaction model with remote sensors and field data

Angus I. Calderhead
Institut National de la Recherche Scientifique, University of Quebec, Québec, Québec, Canada
Richard Martel
Institut National de la Recherche Scientifique, University of Quebec, Québec, Québec, Canada
Alfonso Rivera
Geological Survey of Canada, Natural Resources Canada, 490 de la Couronne, Quebec, QC Canada
René Therrien
Département de géologie et de génie géologique, Université Laval, Québec, QC G1K 7P4, Canada
Jaime Garfias
Centro Interamericano de Recursos del Agua – Universidad Autónoma del Estado de México, Toluca, State of Mexico, México

ABSTRACT
The Toluca Valley, Mexico experiences heavy groundwater pumping and significant land subsidence. This study examines pumping induced regional land subsidence of the Toluca Valley. The study is divided as follows: (1) obtaining remote sensing data, field data, and all available literature for the Toluca Valley; (2) coupling compaction to the groundwater flow equation with the HGS model; and (3) constraining the model with available data to eventually examine several pumping scenarios for minimizing future land subsidence. It is apparent that continuing at the current rates of the water consumption will lead to more subsidence. Average estimates predict a maximum subsidence in the valley that will reach 1.2 m in the next 40 years.

RÉSUMÉ
La Valle de Toluca, Mexique subit un pompage d'eau souterraine et connaît un problème de subsidence important. Cette étude examine l'affaissement des sols résultant de l'extraction d'eau souterraine dans la vallée de Toluca. L'étude se divise par (1) obtenir toutes les données (satellitaire, terrain, littérature) disponibles; (2) coupler la compaction a l'équation d'écoulement avec HydroGeoSphere; (3) contraindre le modèle avec les données disponibles et examiner plusieurs scenarios pour minimiser l'affaissement à venir. Il est évident que si l'on continue au taux de consommation d'eau présente, il y aura d'avantage d'affaissement. Les prédictions moyennes estimes que l'affaissement maximal dans la vallée sera environs 1.2 m dans les prochaines 40 années.

1 INTRODUCTION

In many urban settings, excessive groundwater pumping from aquifers composed of compressible clays leads to land subsidence, potentially causing significant damage to buildings and infrastructure.

Numerical models serve as important tool in analysing subsidence patterns. Terzhaghi's 1D effective stress principle coupled to groundwater flow has most recently been applied by Hoffmann et al. (2003), Leake and Galloway (2007), and Lui and Helm (2008). The objective of this study is to examine land subsidence occurrences in the Toluca Valley, Mexico. A newly coupled finite element 1-D instantaneous compaction and 3D groundwater flow model, Hydrogeosphere (HGS) (Therrien et al., 2009) is used for the analysis. The model is coupled, verified and then applied to the Toluca Valley. Field data, remote sensing techniques, and available literature are used for constraining the new model, and finally several pumping scenarios for minimizing future land subsidence are examined.

The Toluca Valley presently exports 38% (6m^3/s) of its groundwater resources to Mexico City (CNA, 2007). The Toluca Valley's water resource and land subsidence problems are of interest because the basin was formally seen as an important source of water to the Mexico City basin, yet today the Toluca Valley can no longer support its own growth let alone provide for Mexico City's. Inter-basin water transfer is examined as both a problem (exports) and a solution (imports) to the ongoing subsidence.

In contrast to Mexico City's well documented subsidence, very little compaction information has been documented in the Toluca Valley even though subsidence occurrences have been noticed since the early 1970's. Remote sensing information (Synthetic Aperture Radar (SAR) images) in the last 10 years has added to the overall understanding of the subsidence occurrences.

2 COMPACTION BACKGROUND

According to Terzaghi (1925) (equation 1), changes in the effective stress can result from changes in the total stress or changes in pore pressure. The total stress is given by the geostatic load of the overlying saturated and unsaturated sediments.

$$\sigma'_{ij} = \sigma_{ij} - p \quad (1)$$

where

σ'_{ij} is a component of the effective stress tensor,
σ_{ij} is a component of the total stress tensor, and
p is the fluid pore pressure.

A change in effective stress resulting from a given head change generally differs in confined and unconfined aquifers. In an unconfined aquifer, a change in head corresponds to a draining or re-wetting of pore space and results in a change in the geostatic load or the total stress on the underlying sediments as well as the pore pressure. The change in effective stress caused by a head change in the saturated portion of an unconfined aquifer can be described as (Poland and Davis, 1969):

$$\Delta\sigma'_{zz} = -\rho_w g (1 - n + n_w) \Delta h \quad (2)$$

where

$\Delta\sigma'_{zz}$ = the change in vertical effective stress (positive for increase),
n = the aquifer porosity,
n_w = the moisture content in the unsaturated zone above the water table, as a fraction of total volume, and
Δh = the change in hydraulic head.

It should be noted that changes in head in an unconfined aquifer constitute a mass change in that aquifer. This represents a change in the total stress for all underlying confined aquifers. In a confined aquifer, the total stress changes negligibly with changes in pore pressure as water is released from or is taken into storage by the saturated porous medium as a result of the compression or expansion of the medium and (or) the water. The change in water density associated with the expansion or compression of the water is negligible. Thus the change in effective stress for a given change in head can be expressed as (Poland and Davis, 1969)

$$\Delta\sigma'_{zz} = -\rho_w g \Delta h \quad (3)$$

In Hydrogeosphere the compaction module is designed to simulate instantaneous compaction and storage changes in confined aquifer systems and is thus based on equation 3. For compressible layers in the saturated part of an unconfined aquifer where hydraulic-head variations are occurring, this approach will overestimate the change in effective stress, and thus overestimate sediment compaction by the factor $(1 - n + n_w)^{-1}$ (see Equation 2).

Changes in effective stress ($\Delta\sigma'_{zz}$) cause compaction and expansion of the sediments constituting many aquifer systems. In this paper, the term compaction is used to describe a reduction in the thickness of a horizontal compressible layer. A negative compaction implies an expansion or increased thickness of the compressible layer. Removing horizontal displacements, the one-dimensional compressibility ($\overline{\alpha}$) can be defined as

$$\overline{\alpha} = \frac{-\frac{db}{b}}{d\sigma'_{zz}} \quad (4)$$

where

db is the change in thickness of a control volume with initial thickness b.

If the change in effective stress is due only to a change in the pore pressure, equation 3 can be used to express equation 4 as:

$$\rho_w g \overline{\alpha} b = S'_{sk}\, b = S'_k = \frac{db}{dh} \quad (5)$$

where

S'_{sk} is $\rho_w g \overline{\alpha}$, the skeletal specific storage
S'_k is $S'_{sk}b$, the skeletal storage coefficient, and
dh is the change in hydraulic head.

Laboratory consolidation tests on sediment cores and measurements of aquifer-system compaction obtained from borehole extensometers indicate that the compressibility, and thus the skeletal specific storage, can assume very different values depending on whether or not the effective stress exceeds the previous maximum effective stress, termed the preconsolidation stress (Johnson and others, 1968; Riley, 1969; Jorgensen, 1980).

For some sediments inelastic compaction is approximately proportional to the logarithm of the effective stress (Jorgensen, 1980). However, in many cases applicable to aquifer-system compaction where incremental changes in effective stress are typically small (e.g. the Toluca Valley), the relationship (equation 5) can be linearized as

$$\Delta b = S'_k\, \Delta h \quad (6)$$

where:

Δb is the change in thickness of the sediment layer
S'_k is the skeletal storage coefficient
Δh is the change in hydraulic head

To account for the marked change of the skeletal specific storage when the effective stress exceeds the preconsolidation stress, two separate values are often used:

$$S'_k = \begin{cases} S'_{ske} & for\ \sigma'_{zz} < \sigma'_{zz(pre)} \\ S'_{skv} & for\ \sigma'_{zz} \geq \sigma'_{zz(pre)} \end{cases} \quad (7)$$

where:

S'_{ske} is the elastic skeletal specific storage,

S'_{skv} is the inelastic, or virgin, skeletal specific storage, and $\sigma'_{zz\,(pre)}$ is the preconsolidation effective stress.

3 METHODOLOGY

3.1 Toluca Valley data

The Toluca Valley basin (Figures 1) covers an area of approximately 2100 Km^2. The basin is adjacent to the Mexico City Valley, with the Sierra Las Cruces forming a natural border between the two basins. The Toluca Valley's geographic position in the center of the country and proximity to Mexico City, as well as its rapidly developing infrastructure, have allowed the city to grow into a major industrial zone for the country.

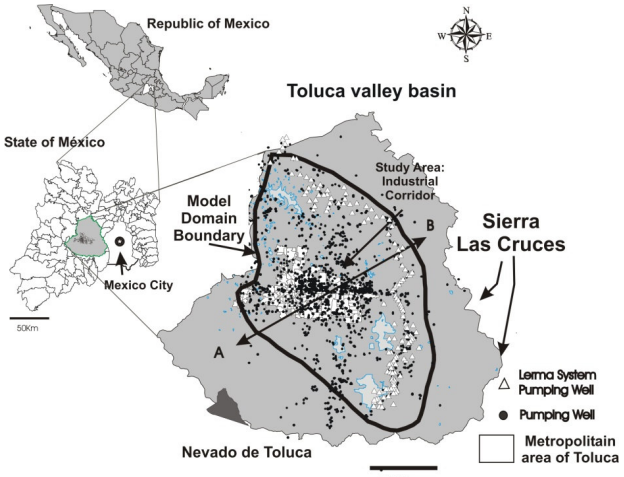

Figure 1: Location map of the Toluca Valley and model domain boundary within the Republic of Mexico and the State of Mexico. Over 935 pumping wells are in operation in the Valley, including the 230 Lerma system wells that are located along the Lerma river on the eastern edge of the valley.

Heavy groundwater pumping for local use and exports to Mexico City have caused a significant groundwater deficit over the last 45 years. A comprehensive recharge and discharge model (Calderhead et al. 2009a) shows that the deficit will continue to increase (Figure 2).

Very little compaction data was available from the literature thus efforts were made to obtain subsidence data from two bore holes equipped with one extensometer each and from D-InSAR subsidence maps.

Extensometers

The objective of installing the extensometers was to obtain accurate field measurements at point locations. Two R-4 magnetic reed switch probe extensometer systems by Roctest® (Roctest, 2009) were installed in the Industrial Corridor (Figure 4A). Boreholes with a 15 cm diameter were bored by a rotary drill and reach 115 and 78 meters depth respectively for Extensometer-1 and Exsensometer-2. For this study, reading frequencies from the extensometers varied from 1 to 6 months and spanned two years beginning in July of 2006 and ending in July of 2008.

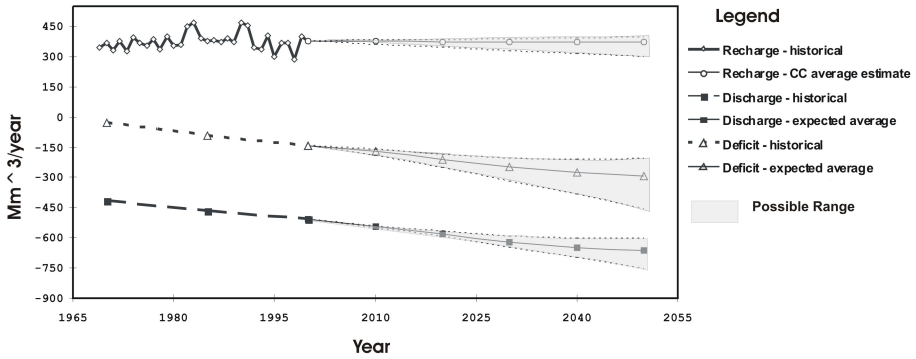

Figure 2: Observed and expected groundwater recharge, pumping, and deficit from 1970 to 2050. From 1970 to 1999 actual recharge values are shown. From 2000 to 2050 average expected recharge including climate change (IPCC, 2007) is shown. Recharge, discharge and deficit projections are based on Calderhead et al. (2009a). The deficit is the sum of the recharge and the discharge. Modified from Calderhead et al. (2009a)

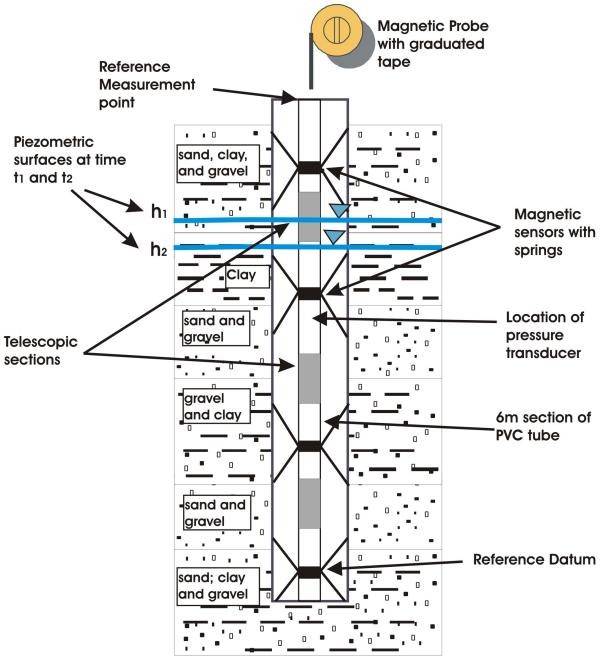

Figure 3: Schematic drawing of the magnetic probe extensometer. Piezometric surface variations with time and location of pressure transducer are also represented. Drawing is not to scale.

D-InSAR

Over the last two decades, the immergence of differential synthetic aperture radar interferometry (D-InSAR) as a tool for monitoring land movement, at the regional scale with sub-centimeter vertical precision, has revolutionized subsidence studies. D-InSAR provides the possibility to calibrate subsidence models even with little field subsidence data available.

InSAR derived subsidence maps are used to constrain the compaction model. The interferograms and deformation maps are useful for locating compacting regions and quantifying subsidence magnitudes. SAR images were obtained from ERS-1, ENVISAT ASAR, and RADARSAT-1 between 1996 and 2008 (Table 1). Calderhead et al. (2009b) presents the complete InSAR results for the Toluca Valley. Table 2 summarises the 31 interferograms used to derive compaction rates.

Figure 4A shows pumping occurrences overlaying the aggregate clay thickness; and Figure 4B is a representative D-InSAR interferogram of the entire valley showing localized subsidence zones over a 70 day period. From Figure 4B, there is very limited coherence in the North-East and South-West corners, thus limiting its usefulness. However, usable results are obtained throughout the central part of the valley. Note that the interferogram is not optimised for parameter retrieval in zone E; this zone of maximum subsidence is studied in more detail in the results section. For the 70 days between December 5th and February 13th, zones A though G are 'hotspots' with very clear subsidence patterns observed. If one observes the zoom on zone A (Figure 4B), two colour cycles (clockwise: yellow-blue-red; see legend of Figure 4B) are observed and represent a total subsidence of 56 mm for the given period. This translates to subsidence rates of 29 cm/year. However, as noted by Calderhead et al.'s (2009b) D-InSAR study of the Toluca Valley, depending on the geological context and the pumping rates, the maximum subsidence rates are often variable in space, time, and magnitude.

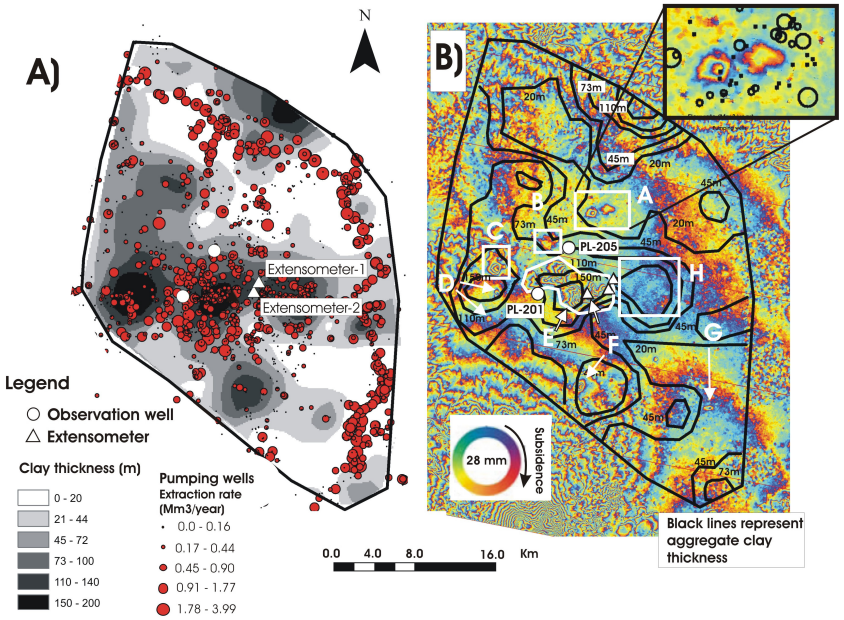

Figure 4: A) Aggregate clay thickness and pumping occurrences B) Differential Interferogram of the Toluca Valley with a time interval of 70 days. ENVISAT ASAR images were acquired on December 5th 2007 and February 13, 2008. Lines of equal aggregate thickness are overlain also shown on the map.

Figure 4A shows pumping occurrences overlaying the aggregate clay thickness; and Figure 4B is a representative D-InSAR interferogram of the entire valley showing localized subsidence zones over a 70 day period. From Figure 4B, there is very limited coherence in the North-East and South-West corners, thus limiting its usefulness. However, usable results are obtained throughout the central part of the valley. Note that the interferogram is not optimised for parameter retrieval in zone E; this zone of maximum subsidence is studied in more detail in the results section. For the 70 days between December 5th and February 13th, zones A though G are 'hotspots' with very clear subsidence patterns observed. If one observes the zoom on zone A (Figure 4B), two colour cycles (clockwise: yellow-blue-red; see legend of Figure 4B) are observed and represent a total subsidence of 56 mm for the given period. This translates to subsidence rates of 29 cm/year. However, as noted by Calderhead et al.'s (2009b) D-InSAR study of the Toluca Valley, depending on the geological context and the pumping rates, the maximum subsidence rates are often variable in space, time, and magnitude.

3.2 Coupling Compaction to groundwater flow

With the objective of representing land subsidence in the Toluca Valley, Mexico, a compaction module was added to the multipurpose 3D finite element groundwater flow model HGS. The following equation is used to describe HGS`s modified version of three-dimensional transient subsurface flow for a fully saturated porous medium (Therrien et al., 2009):

$$-\nabla q + \sum \Gamma_{ex} \pm Q = S_s \frac{\partial h}{\partial t} \qquad (8)$$

with the fluid flux q given by:

$$q = -K \nabla h \qquad (9)$$

and the hydraulic head h. The hydraulic conductivity, K, is given by:

$$K = \frac{\rho_w g}{\mu} k \qquad (10)$$

where g is the gravitational acceleration constant, μ is the viscosity of water, k is the permeability tensor of the porous medium and ρ is the density of water.

Fluid exchange with the outside of the simulation domain, as specified from boundary conditions, is represented by Q, In Equation 8, Γ_{ex} represents the volumetric fluid exchange rate between the subsurface domain and all other types of domains supported by the HGS model and it is expressed per unit volume of the other domain types. The definition of Γ_{ex} (positive for flow into the porous medium) depends on the conceptualization of fluid exchange between the domains.

If the aquifer system includes compressible sediments, this term can be multiplied by $(1 - \gamma^*)$, where γ^* is the fraction, by volume, of compressible interbeds in the aquifer system.

Thus, combining the compaction term to the governing equation yields: (11)

$$-\nabla \cdot q + \sum \Gamma_{ex} \pm Q = \left[(1-\gamma^*) * S_s + \gamma^* * S'_{sk}\right] \frac{\partial h}{\partial t}$$

4 RESULTS

Simulating the hydraulic head involved using hydraulic head values from multilevel piezometers located throughout the valley. More detail was placed on the industrial corridor where the largest drawdowns are observed. The simulated hydraulic head at Extensometer 1 follows the general hydraulic head pattern of PL-201, PL-205, and Extensometer 1 (Figure 5).

At the Extensometer-1 location, similar subsidence patterns are observed from ENVISAT ASAR, RADARSAT-1, Extensometer-1, and the HGS compaction simulation (Figure 6). Assuming instantaneous

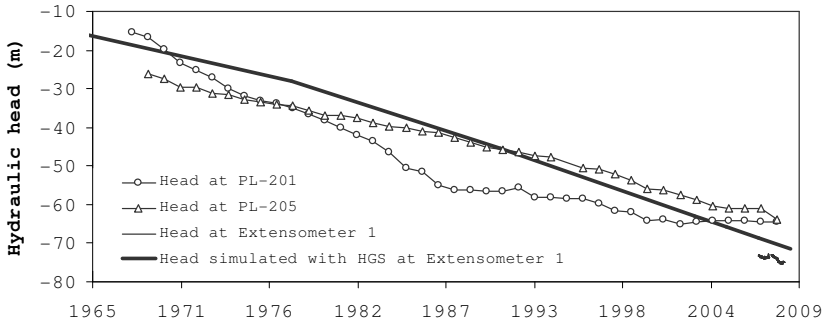

Figure 5: Measured and simulated hydraulic head values at Extensometer 1 contrasted with nearby long term monitoring wells PL-201 and PL-205

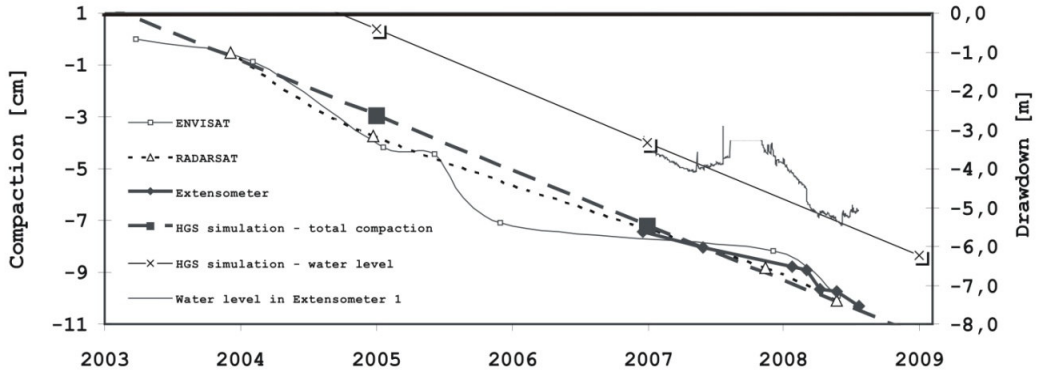

Figure 6: Simulated and measured total compaction at Extensometer 1 by ENVISAT ASAR, RADARSAT-1, Extensometer-1, and HGS simulation. Simulated and measured hydraulic head at Extensometer-1 are also included.

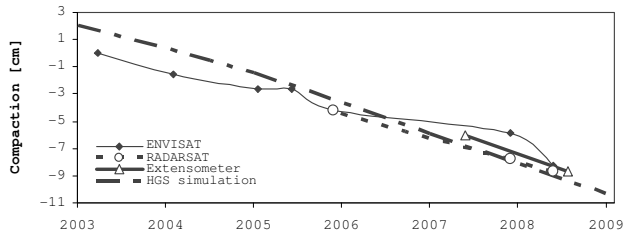

Figure 7: Subsidence at the Extensometer 2 location measured by ENVISAT ASAR, RADARSAT-1, Extensometer 2, and HGS between March 2003 and May 2008.

compaction, approximately 1 metre of drawdown leads to 1 cm of compaction. Subsidence at Extensometer-2 is observed in Figure 7. The extensometer data slope coincides relatively well with the D-InSAR results and the numerical model. The order of subsidence is similar to Extensometer-1's values with approximately 9 cm of compaction between November 2003 and May 2008. Considering the proximity of Extensometer 2 to Extensometer 1, hydraulic head decline is assumed to decrease at a similar rate to Extensometer 1 (Figure 6). Considering head decline, compaction magnitudes are similar for both locations; the total skeletal specific storage values are also assumed to be similar.

Scenarios 1-3 (Table 2) examine worst case, best case, and average expected values based on table 1. Recharge and discharge are assigned with their respective scenario based on table 1 with pumping divided into (A) exports to Mexico City and (B) local use. Exports to Mexico City are expected to increase (8 m^3/s) in the worst case scenario, decrease (3 m^3/s) in the best case scenario and remain constant (6 m^3/s) in the average expected scenario.

A probable scenario is that pumping to Mexico City decreases thus scenarios 4 and 5 decrease exports to 0 m^3/s and 3 m^3/s respectively while keeping average estimates for all other parameters. Scenario 6 examines the possibility of decreasing pumping in Toluca (-25%) and Mexico City (-50%) to a more sustainable rate. Scenarios 7 and 8 make use of the clay thickness model (Figure 4A) for moving pumping wells in areas with high clay content to areas with lower clay content. Scenario 7 assumes average expected pumping and scenario 8 decreases pumping rates to scenario 6 values. By decreasing pumping for local use within the valley, scenarios 6 and 8 imply inter-basin water transfer from surrounding basins.

Scenario	Lerma pumping (to Mexico City)	Toluca Pumping	Recharge	Description
1	33% increase	worst case	worst case	Worst case expected with 33% increased Lerma pumping
2	50% decrease	best case	best case	Best case expected with 50% decrease in Lerma
3	constant at 6m3/s	average	average case	Average case with Lerma pumping constant at 6m3/s
4	Stop Lerma pumping (0m3/s)	average	average case	Average case with stopping Lerma pumping
5	50% decrease	average	average case	Average case with a 50% decrease in Lerma pumping
6	50% decrease	decrease by 25%	average case	Decrease Lerma pumping by 50% and decrease Toluca Basin pumping by 25%
7	constant at 6m3/s	average	average case	Move pumping centres to locations with less clay
8	50% decrease	decrease by 25%	average case	Move pumping centres to locations with less clay and decrease Toluca Basin pumping by 25% and Lerma Pumping by 50%

Table 2: Pumping scenarios 2010-2050

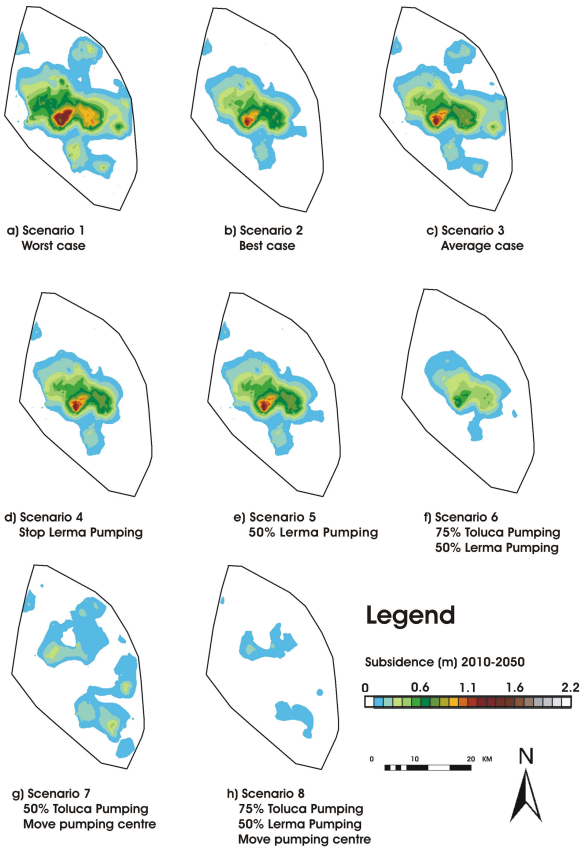

Figure 8: Subsidence scenarios 2010-2050 (see Figure 1 for location of the simulated domain)

Figure 8 presents the total compaction results between 2010 and 2050 for the 8 scenarios. Maximum total subsidence reaches 2.2 m for the worst case scenario (scenario 1), 1.4 m for the best case scenario (scenario 2), and 1.6 m for the average expected subsidence (scenario 3). Comparing scenarios 3, 4 and 5 is of interest. There are only subtle differences between stopping exports (scenario 4) and cutting exports in half (scenario 5). However, there are noticeable differences between constant exports (scenario 3) and cutting exports in half (scenario 5).

The most marked change in subsidence occurs when moving the pumping centres (scenarios 7 and 8) away from compressible clays. Total compaction can be drastically reduced by simply moving the pumping centres to different locations within the valley. The most desirable results (scenario 8) show a localized maximum subsidence of < 0.3 m in 2050, otherwise there is only limited subsidence throughout the valley.

5 DISCUSSSION AND CONCLUSION

Limitations exist for the new HGS-compaction numerical model in representing subsidence. Using the linearized form of the constitutive law introduces errors into the calculations (Narasimhan and Witherspoon, 1977, and Bethke and Corbett, 1988). Leake and Prudic (1991) have estimated the error of this method by comparing the linearized equations of computed compaction with a more complex treatment of computed compaction using S'_{skv} proportional to log σ'_{zz}. Their results indicate that using the linearized form overestimates compaction by about one-half the percentage increase in effective stress. Hoffman et al. (2003) estimates that if the effective stress increases by 10 percent, compaction would be overestimated by about 5 percent. For sediments relatively deep below the land surface, a given decline in head will result in a smaller percentage increase in effective stress than for shallower sediments. The new HGS-compaction code gives very reasonable estimates for instantaneous subsidence in confined aquifers, however there is room for improving the estimates by including aspects such as dependence on hydraulic conductivity, non-linear deformation, time delays, effects of moving water tables, and extending to a 3D representation of deformation.

The D-InSAR data was very useful in calibrating the subsidence model. InSAR has a large potential for mapping subsidence. With a steady increase in the number of InSAR capable satellites becoming available, more data and software will become available. As mentioned by Calderhead et al. (2009b), several factors influence the suitability of InSAR use for deformation mapping: 1- Perpendicular baselines between satellite acquisitions have upper limits (generally < 600 m); 2- atmospheric effects: spatial variability of the atmosphere changes with time thus fringes are produced by atmospheric effects; 3- temporal decorrelation: vegetation growth or movement is a common cause for InSAR decorrelation; 4- Resolution of the sensors and the DEM: higher spatial resolution leads to more accurate results; 5- band type and wavelength – the band type of the sensor can be a factor in obtaining usable results.

It is apparent that continuing at the current rates of water consumption will lead to more subsidence. Even in the best case scenario (scenario 2), maximum subsidence occurrences over a 40 year period will reach 1.4 m.

Considering that the Lerma pumping system is mostly located in regions with low clay content and little difference is observed between scenarios 4 and 5, completely stopping exports to Mexico City (scenario 4) is not necessary for controlling the subsidence. However, decreasing exports by half (scenarios 2, 5, 6, and 8) does have a positive effect on the overall water budget and subsidence. It can be argued that all scenarios will require inter-basin water transfer at a later date because the water budget deficit is not sustainable.

Inter-basin water transfer alone is not sufficient for controlling the subsidence. It is shown that the best way of controlling subsidence is by relocating the pumping centres to other locations with low clay content. Had a pumping system been in place to pump water to the urbanized part of the valley (scenarios 7 and 8), much of the land subsidence could have been avoided. Even if

scenarios 7 and 8 are not undertaken, when planning water imports to the Toluca Valley from other basins, one can learn from past mistakes and avoid drilling new wells in locations with thick compressible clay units - whether for exporting or local use.

ACKNOWLEDGEMENTS

We are thankful to the Ministère des Relations Internationales du Quebec, CONACyT, the Autonomous University of the State of México (UAEM), INRS-ETE, NSERC (a discovery grant held by Richard Martel), AUCC/IDRC, and the Ministère d'Éducation du Québec for their financial support. We are appreciative of Sergio Murillo from the Comision National del Agua for logistical support on the field. We are grateful to the Canadian Space Agency and the Geological Survey of Canada for providing the RADARSAT-1 data and finally, we acknowledge the European Space Agency`s contribution for providing ERS and ENVISAT ASAR data at cost of reproduction under project C1P 3821.

REFERENCES

Bethke, C.M., and Corbett, T.F., 1988. Linear and nonlinear solutions for one-dimensional compaction flow in sedimentary basins: Water Resources Research, v. 24, p. 461–467.

Calderhead A. I., Martel, R. Rivera, A., Garfias, J., Therrien, R., 2009a. An increasing groundwater budget deficit induced by urbanization, industrialization, and climate change in the Toluca Valley, Mexico. Journal of hydrology (Submitted)

Calderhead, A. I., Martel, R., Allasset, P-J., Rivera, A., Garfias, J,. 2009b. Land subsidence induced by groundwater pumping, monitored by C-band D-InSAR and field data in the Toluca Valley, Mexico. International Journal of Remote Sensing (Submitted)

CNA, 2007. Base Aquiferos Nacional y Regional. Comisión Nacional del Agua- database.

Galloway, D.L. and Hoffmann J. 2007 The application of satellite differential SAR interferometry-derived ground displacements in hydrogeology. Hydrogeology Journal (2007) 15: 133–154

Hoffmann J, Leake SA, Galloway DL, Wilson AM, 2003. MODFLOW-2000 ground-water model-user guide to the subsidence and aquifer-system compaction (SUB) package. USGS Open-File Rep 03-233.

IMTA, 2003. Censo del utilización del agua en el valle de Toluca. Instituto Mexicano de Tecnologia del Agua.

INEGI, 2009. Instituto Nacional de Estadística, Geografía e Informática, Sinthesis of geographic information for the state of Mexico. Aportación al Producto Interno Bruto (PIB) nacional/ Contribution to Gross Domestic Product (GDP)http://cuentame.inegi.org.mx

IPCC, 2007. Climate Change 2007: The Physical Science Basis. Contribution of Working Group I to the Fourth Assessment Report of the Intergovernmental Panel on Climate Change [Solomon, S., D. Qin, M. Manning (eds.)].

Johnson, A.I., Moston, R.P., and Morris, D.A. 1968. Physical and hydrologic properties of water-bearing deposits in subsiding areas in California: U.S. Geological Survey Professional Paper 497-A, 71 p.

Jorgensen, D.G., 1980. Relationships between basic soils-engineering equations and basic ground-water flow equations: U.S. Geological Survey Water-Supply Paper 2064, 40 p.

Leake, S.A., and Prudic, D.E., 1991. Documentation of a computer program to simulate aquifer-system compaction using the modular finite-difference ground-water flow model: U.S. Geological Survey Techniques of Water-Resources Investigations, book 6, chap. A2, 68 p.

Leake, S.A., and Galloway, D.L., 2007. MODFLOW ground-water model—User guide to the Subsidence and Aquifer-System Compaction Package (SUB-WT) for water-table aquifers: U.S. Geological Survey, Techniques and Methods 6–A23, 42 p.

Legorrreta, J., 1997. Rainfall, the key to the future of the Valley of Mexico. *La Jornada Ecologica*, **5**(58): 1-12.

Liu, Y., and D. C. Helm 2008., Inverse procedure for calibrating parameters that control land subsidence caused by subsurface fluid withdrawal: 1. Methods, *Water Resour. Res*., 44, W07423, doi:10.1029/2007WR006605.

Narasimhan, T.N., and Witherspoon, P. A. 1977. Numerical model for land subsidence in shallow ground-water systems, Internat. Assoc. Sci. Hydrology Pub. 121, p. 133-144.

Poland, J.F., and Davis, G.H., 1969. Land subsidence due to withdrawals of fluids, *in* Varnes, D.J., and Kiersch, G., eds.: Geological Society of America Reviews in Engineering Geology, v. 2, p. 187–269.

Riley, F.S., 1969. Analysis of borehole extensometer data from central California: International Association of Scientific Hydrology Publication 89, p. 423–431.

Roctest, 2009. R-4 magnetic reed switch probe extensometer system, Roctest http://www.roctest.com/modules/AxialRealisation/img_repository/files/documents/R4-E5013D-W.pdf

Terzaghi, K. 1925. Earthworks mechanics based on soil physics. Erdbaumechanik auf bodenphysikalisher Grundlage, Franz Deuticke, Vienna

Therrien, R., McLaren, .G. Sudicky, E.A., Panday, S.M. 2009 User Guide: HydroGeoSphere - A Three-dimensional Numerical Model Describing Fully-integrated Subsurface and Surface Flow and Solute Transport